FORMATION FLYING RECONFIGURATION MANOEUVRES VIA ENVIRONMENTAL FORCES IN HIGHLY ELLIPTICAL ORBITS

Rebecca La Norcia[a,*], Dario Spiller[b], Christian Circi[c], Fabio Curti[d]

[a] *M.Sc. Graduate, School of Aerospace Engineering, Sapienza University of Rome, Via Salaria 851, 00138 Rome, Italy*
[b] *PostDoc, School of Aerospace Engineering, Sapienza University of Rome, Via Salaria 851, 00138 Rome, Italy*
[c] *Associate Professor, Department of Astronautical, Electrical and Energy Engineering, Sapienza University of Rome, Via Salaria 851, 00138 Rome, Italy*
[d] *Associate Professor, School of Aerospace Engineering, Sapienza University of Rome, Via Salaria 851, 00138 Rome, Italy*

Abstract

A study on reconfiguration manoevres applied to a tetrahedral formation in highly elliptical orbits is proposed, by using a propellantless solution. The manoeuvring strategy consists in exploiting certain environmental forces, specifically those provided by solar radiation pressure and atmospheric drag, by actively controlling the satellites' attitudes. Through inverse dynamics particle swarm optimization the optimal attitudes required for the manoeuvres are evaluated, whereas the configuration's evolution is simulated by a high-fidelity orbital simulator. The goal of the reconfiguration problem is to find an optimal control in order for the four spacecraft to reach a desired configuration in a specified portion of orbit, where the desired configuration is evaluated by a shape and size geometric parameter. By increasing the manoeuvring time and the satellites' area to mass ratio, possible solutions to the limitations concerning the proposed manoeuvring approach are verified.

Keywords: Formation Flying, Highly Elliptical Orbits, Simulation and

*Corresponding author
Email addresses: rebecca.lanorcia@gmail.com (Rebecca La Norcia), dario.spiller@uniroma1.it (Dario Spiller), christian.circi@uniroma1.it (Christian Circi), fabio.curti@uniroma1.it (Fabio Curti)

1. Introduction

One of the biggest challenges when dealing with satellites in formation flying is to ensure that the configuration satisfies certain conditions in terms of the satellites' position and attitude, related mainly to the task of keeping the formation from drifting away, as well as to the mission requirements. At the present time, in order to deal with such challenges on board thrusters are used, chemical and/or electrical, and especially the chemical ones require propellant. Therefore, formation flying satellites require more fuel than stationkeeping a single spacecraft, since the formation maintenance requirements are more demanding, making the task of minimizing the fuel consumption even more important than usual in space missions (Alfriend et al., 2009). For this reason great interest is given in studying propellant-less solutions, such as passive manoeuvres obtained by exploiting certain environmental forces like Solar Radiation Pressure (SRP) and atmospheric drag. This paper investigates the feasibility of achieving passive reconfiguration manoeuvres by using perturbing forces, in the case of a tetrahedral satellite formation configuration in a Highly Elliptical Orbit (HEO), for instants a Molniya type of orbit. This approach is to be considered as an aid to the traditional propellant control solutions. It is thought primarily to reduce the mission's fuel requirements, therefore opening to the possibility of extending the mission's life (for example in the case of HEO such as Molniya orbits or Tundra orbits, a ΔV of approximately 50 m/s per year per satellite is required for station keeping manoeuvres (Konstantinov & Obukhov, 2005) (Bruno & Pernicka, 2005), or as reported in (Armellin et al., 2004) for the case of a low thrust propulsion an average ΔV consumption of 5.1 mm/s is required for each orbit); secondarly, its feasibility can be considered in view of a back-up system in case of a failure in the propulsion system.

In (Reid & Misra, 2011) the effects of aerodynamics forces on formation flying satellites has been investigated, with the purpose of assessing the use of

differential drag as a means of formation maintenance. A feasibility study on the use of differential drag as a way to control a nano-satellite formation is conducted in (Kumar et al., 2011), whereas in Ivanov et al. (2018) the possibility of constructing and maintaining a tetrahedral configuration of four nanosatellites after deployment in LEO is studied. In (Traub et al., 2018) it is possible to find an extensive literature review of the major contributions which led to the current state-of-the-art on the use of atmospheric forces as propellant-less source of control for satellite formation flight, and the major key gaps that need to be addressed in order to enhance the current state-of-the-art. SRP has been studied with the purpose of station keeping manoeuvres in (Oliveira & Prado, 2015) as a way to reduce fuel consumption by finding the necessary and sufficient conditions to use solar sails in order to compensate or to reduce the perturbation effects due to external forces received by a satellite. In (Parsay & Schaub, 2017) and (Parsay et al., 2018) the use of solar sail is investigated with the purpose of precessing the orbit apse lines of satellite in formation flying on an Earth-centered orbit, in a Sun-synchronous way. In (Hou et al., 2016) it is demonstrated that the control of tetrahedron satellite formation flying in a geosynchronous orbit using SRP is feasible, both for formation maintenance and for formation reconfiguration, whereas in (Mashtakov et al., 2018) the possibility of simultaneously controlling both the relative motion and the attitude of satellites in formation flying via SRP is investigated, through solar sails made of a material that is able to change its optical properties. (Williams & Wang, 2002) examines the proper use of a solar wing in order to maintain a desired formation. Several studies have been made on the use of SRP to control formation flying around the L2 libration point in the Sun-Earth system, like the ones conducted by (Shahid & Kumar, 2010, 2014), or by (Li & Williams, 2006) in which reconfiguration of formations near one of the Sun-earth Libration points is examined. In (Kumar et al., 2014) both the SRP and aerodynamic forces are exploited in order to maintain satellite formations by controlling SRP or aerodynamic flaps, although these forces are exploited separately by considering firstly a Low Earth Orbit (LEO) and secondly a geostationary orbit.

The optimal control problem addressed in this study resolves in a control strategy such that, after reconfiguration, the four spacecraft are arranged in order to form an acceptable tetrahedral configuration throughout a portion of orbit around the apogee, referred to as the Region of Interest (ROI). A similar problem is addressed in (Huntington & Rao, 2008), in which the problem is posed as a multi-phase nonlinear optimal control problem solved using the Gauss pseudospectral method, in order to reconfigure a tetrahedral formation in a fuel-optimal manner. Differently from (Huntington & Rao, 2008) in which a propellant solution is adopted, the reconfiguration manoeuvres here considered will be achieved through differential drag and differential SRP: by actively controlling the satellites' attitude it is possible to adequately orient the perturbing forces in order to achieve the desired manoeuvres. By doing so the satellites' orbits are modified thanks to the differential accelerations due to different orientations of the satellites' exposed areas.

The manoeuvring approach proposed in this paper has been already investigated in (Spiller et al., 2017b, 2018) and (Spiller, 2018), where both differential drag and differential SRP are considered as control variables for minimum-time reconfiguration manoeuvres of different satellite formations, such as the Projected Circular Formation (PCF), the General Circular Formation (GCF) and the Along-Track Formation (ATF), in the case of circular orbits. The main difference from these works is the orbit choice for the study of the manoeuvring approach and the formation choice. A HEO, in particular a Molnya type of orbit, has been considered in order to study both the SRP and atmospheric drag as control inputs on the same orbit, which makes this study also different from the previously mentioned ones in which SRP and atmospheric drag are in most of the times analysed as separate cases.

The satellites' optimal attitude reorientation is evaluated by the implemented Inverse Dynamics Particle Swarm Optimization (IPSO), which was extensively validated in previous works and perfectly adapts to the problem here considered (Spiller & Curti, 2015; Spiller et al., 2015, 2017a,b; Spiller, 2018). The attitude kinematics is modelled with improved B-Spline curves, whereas the

orbital dynamics will be simulated through the software developed in (Spiller et al., 2017b), based on a high-fidelity orbital simulator that includes the most influent perturbations acting on the satellites.

Three are the main contributions of this paper to the current state of the art on the matter of formation flying reconfiguration manoeuvres: 1) this study verifies the feasibility of achieving passive reconfiguration manoeuvres in a HEO, by exploiting both SRP and atmospheric drag, 2) through the test cases analysed it was possible to define a limit regarding the manoeuvre realization, due to the orientation of the orbit with respect to the Sun; 3) possible solutions to overcome this limitation are suggested and verified, which consist in increasing the area to mass ratio of the formation's satellites, and extending the manoeuvring time.

The rest of the paper is organized as follows: Section 2 provides a description of the reconfiguration problem that has been addressed in this paper, whereas in Section 3 the reconfiguration strategy adopted to achieve the manoeuvre is described. Details of the implementation of the IPSO are presented in Section 4, followed by a description of the numerical results obtained by the simulations carried out on different test cases in Section 5. Finally in Section 6 conclusive observations and remarks are given.

2. Satellite Formation Flying reconfiguration Problem

Let a tetrahedral configuration of $N_F = 4$ satellites be considered, each identified by the subscript $i \in \{1, ..., N_F\}$. Given an Earth-Centred inertial (ECI) reference frame as reported in Figure 1, and both the Keplerian term and the N_{pert} perturbation forces acting on the satellites, the equation of motion of the i^{th} satellite in the ECI frame is:

$$\ddot{\mathbf{r}}_i = -\frac{\mu}{r_i^3}\mathbf{r}_i + \sum_{j=1}^{N_{pert}} \mathbf{f}_{j,i} \tag{1}$$

where $\mu = 3.986 \cdot 10^{-5}$ km^3/s^2 is the Earth gravitational constant, $\mathbf{r}_i$ is the position's vector of each satellite, $\mathbf{f}_{j,i}$ represent the perturbing forces acting on the satellites. The perturbation forces considered in the dynamic model are:

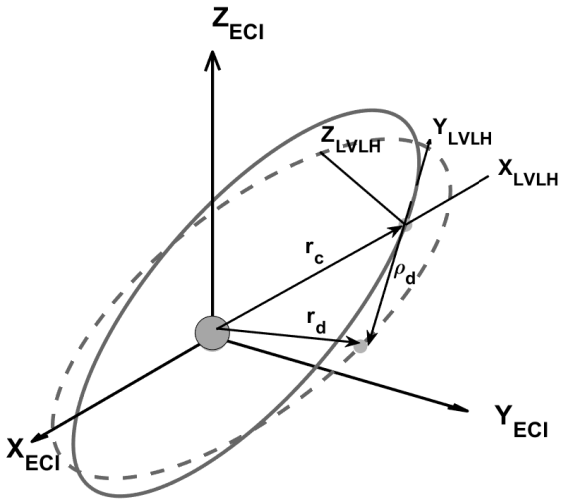

Figure 1: ECI and LVLH refrence systems.

the gravitational harmonics contribution up to the 20^{th} order; third body perturbations from the Sun and the Moon; the Solar Radiation Pressure (SRP); the atmospheric drag, having considered the Jacchia-Roberts atmosphere model (Vallado, 2001). The satellites' relative dynamics are described with respect to the formation's mesocentre (i.e. the geometric centre of the formation). Given the choice of the formation, the mesocentre is not occupied by a physical satellite and it represents the origin of the rotating Local Vertical Local Horizontal (LVLH) reference frame, as represented in Figure 1. The numerical integration of the non-liner dynamics of each satellite is performed on the inertial state. The relative representation of the formation is used only for a posteriori description. The reason for such a choice is related to the fact that the deputies' inertial states have to be integrated in order to define the mesocentre's position, and since the perturbations are taken into account, there are no advantages in expressing the non-linear equations of relative motion in the LVLH frame.

The reference orbit considered to study the configuration's evolution is a

Table 1: Molniya orbital elements.

Parameter	Value	Parameter	Value
a (km)	26600	Ω (deg)	0
e	0.74	ω (deg)	270
i (deg)	63.4	ν_0 (deg)	200

Molniya type of orbit, whose parameters can be found in Table 1. Because of this choice of orbit, both SRP and atmospheric drag are considered as control inputs in order to passively manoeuvre the formation's satellites. The principle of exploiting differential forces is the main feature of the reconfiguration strategy: these perturbations act on the satellites in different ways according to their shape and mass, but more specifically these effects change depending on the satellites' attitudes since the same model is considered for all four satellites of the formation. In order to achieve the desired configuration, these differential forces are exploited by adequately modifying the attitude of each satellite, providing the necessary input to perform the orbital manoeuvre.

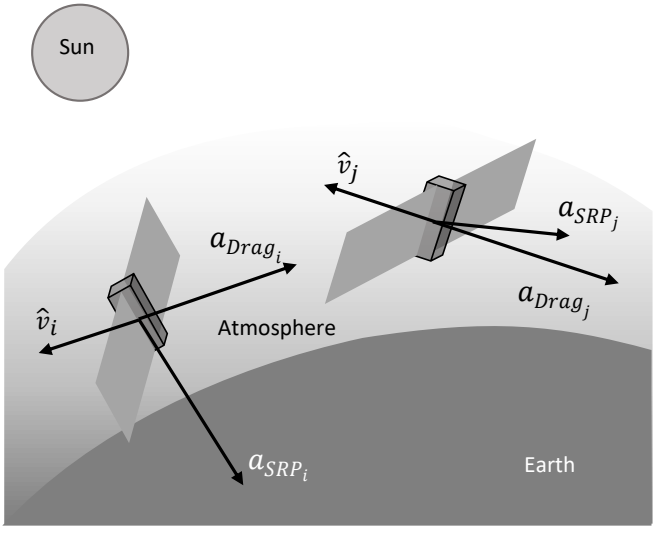

Figure 2: Differential acceleration representation.

By changing the satellites' attitudes, the area of each satellite exposed to the perturbing forces is modified, therefore the intensity and the direction of the specific force due to the exploited perturbation is different from one satellite to another. Differential accelerations, in fact, are defined as the vectorial difference between accelerations acting on two different satellites of the formation, as shown in the explanatory representation in Figure 2. Hence, the differential atmospheric drag acceleration and differential SRP acceleration acting on the $i-th$ satellite with respect to the $j-th$ satellite, can be defined as follows:

$$\begin{aligned} \mathbf{a}_{DD}^{(i,j)} &= \mathbf{a}_{Drag}(\mathbf{r}_i, \dot{\mathbf{r}}_i, \boldsymbol{\xi}_i) - \mathbf{a}_{Drag}(\mathbf{r}_j, \dot{\mathbf{r}}_i, \boldsymbol{\xi}_j), \\ \mathbf{a}_{DSRP}^{(i,j)} &= \mathbf{a}_{SRP}(\mathbf{r}_i, \boldsymbol{\xi}_i) - \mathbf{a}_{SRP}(\mathbf{r}_j, \boldsymbol{\xi}_j) \end{aligned} \tag{2}$$

where $\boldsymbol{\xi}_i$ represents the attitude of each satellite, with $i, j \in \{1, 2, 3, 4\}$ and $i \neq j$.

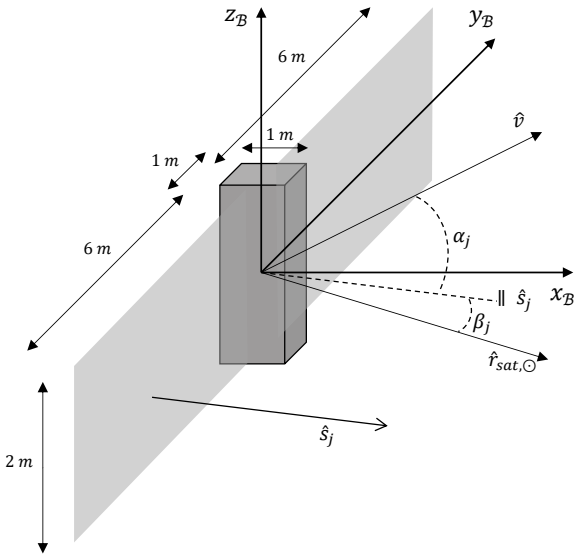

Figure 3: Satellite's model.

With reference to Figure 3, representing the satellite model which is considered equal for all four spacecraft and where the body reference frame $\mathcal{B} =$

$\{x_{\mathcal{B}}, y_{\mathcal{B}}, z_{\mathcal{B}}\}$ is shown, it is possible to define the total accelerations due to atmospheric drag and SRP, acting on each satellite, as follows:

$$\mathbf{a}_{Drag}(\mathbf{r}, \dot{\mathbf{r}}_i, \boldsymbol{\xi}) = -\frac{1}{2} C_D \frac{\sum_{j:\alpha_j < \frac{\pi}{2}} (S_j \cos \alpha_j(\boldsymbol{\xi}))}{m} \rho(\mathbf{r}) \dot{r}^2 \hat{\mathbf{v}} \tag{3}$$

$$\mathbf{a}_{SRP}(\mathbf{r}, \boldsymbol{\xi}) = 2\zeta\gamma \frac{S_0}{mc} \frac{||\mathbf{r}_{\oplus,\odot}||}{||\mathbf{r}_{\oplus,\odot} - \mathbf{r}||} \sum_{j:\beta_j < \frac{\pi}{2}} (S_j \cos^2(\beta_j) \hat{\mathbf{s}}_\mathbf{j}) \tag{4}$$

The unit vector $\hat{\mathbf{v}}$ represents the normalized velocity of the satellite, whereas the unit vector $\hat{\mathbf{s}}_j(\boldsymbol{\xi})$ represents the normal to each j^{th} surface S_j of the satellite, leaving $\alpha_j(\boldsymbol{\xi})$ to be the angle in between. The angle $\beta(\boldsymbol{\xi})$ instead is the angle that each of the satellite's surfaces make with the direction of the solar radiation flux $\hat{\mathbf{r}}_{sat,\odot}$, defined as going from the satellite to the Sun. Both these angles are defined as in the following equations:

$$\alpha_j(\boldsymbol{\xi}) = \cos^{-1}(\hat{\boldsymbol{s}}_\boldsymbol{j}(\boldsymbol{\xi}) \cdot \hat{\mathbf{v}}) \tag{5}$$

$$\beta_j(\boldsymbol{\xi}) = \cos^{-1}(\hat{\mathbf{s}}_\mathbf{j}(\boldsymbol{\xi}) \cdot \hat{\mathbf{r}}_{sat,\odot}) \tag{6}$$

The remaining terms in Eq. (3) and (4) are: the drag coefficient C_D, the satellite mass m, the shadow function ζ, that takes into account umbra, light and penumbra conditions of the satellite, taking on the values of 1 when the satellite is outside the Earth shadow cone, 0 when it is inside and 0.5 when it is in penumbra; the reflectivity coefficient γ; the solar constant $S_0 = 1352,098$ kg/s^2 and the speed of light $c = 2.988 \cdot 10^5$ km/s. The estimation of the density $\rho(\mathbf{r})$ is carried out considering the Jacchia-Roberts model, which offers a reasonable description with a moderate computational expense (Montenbruck & Gill, 2012), which is already sufficiently costly for the problem addressed in this paper. Even more sophisticated models have uncertainties in the density estimation, so there is no reason to implement a more complicated model, considering also the fact that the satellites experience the drag for a very short time compared to the entire orbital period.

The objective behind the study of the reconfiguration manoeuvres is to obtain a regular tetrahedron configuration in a specific region around the apogee of

the reference orbit, defined as the Region of Interest (ROI) (Huntington & Rao, 2008). In order to have a regular tetrahedron configuration, the four spacecraft have to be equally spaced, meaning that the distance between each pair of spacecraft has to be the same. The goal is to control an initial degraded tetrahedral formation in order to satisfy the size and shape requirements in the ROI. The ideal regular tetrahedral shape configuration is set with a 10 km side length, where the formation regularity is evaluated by a geometric quality factor defined similarly to the ones described in (Hughes, 2003; Guzman & Schiff, 2002) and (Mailhe et al., 2000). The quality factor used to evaluate the configuration is a shape and size dependent parameter characterized as follows:

$$Q = \frac{V}{V^*} \cdot Q_S(\bar{L}) \tag{7}$$

where V is the actual volume of the tetrahedral formation and V^* is the volume of the ideal regular tetrahedron calculated considering a 10 km ideal side length. In this way V^* is a constant parameter, whereas in the aforementioned references the same parameter V^* is defined as the volume of a regular tetrahedron with its sides equal to the average side length of the actual tetrahedron. This slight difference in the definition of the quality factor is justified by the fact that the ROI considered in this paper is not so extended, therefore the ideal tetrahedral shape does not change that much in this portion of orbit, simplifying the analysis of the reconfiguration problem here presented.

The term $Q_S(\bar{L})$, in the previous equation, is a function that takes into account the size of the tetrahedron and it is defined as:

$$Q_S(\bar{L}) = \begin{cases} 0 & \bar{L} < l_1 \\ (\bar{L} - l_1)^2 \frac{(\bar{L}+l_1-2l_2)^2}{(l_2-l_1)^4} & l_1 \leq \bar{L} < l_2 \\ 1 & l_2 \leq \bar{L} < l_3 \\ (\bar{L} - l_4)^2 \frac{(\bar{L}+l_4-2l_3)^2}{(l_4-l_3)^4} & l_3 \leq \bar{L} < l_4 \\ 0 & \bar{L} > l_4 \end{cases} \tag{8}$$

where $\bar{L}$ is the average length of the tetrahedron side, $l_1 = 4$ km, $l_2 = 6$ km, $l_3 = 18$ km and $l_4 = 20$ km. The function Q_S is designed accordingly to the

ideal value of the tetrahedron side length. Consequently the function is zero when the average side is far from the nominal value and one when it is in the admissible range.

2.1. Problem Statement

The optimization problem considered here consists in finding the best satellites' attitudes orientations, in order to adequately manoeuvre the formation so as to satisfy the geometric requirements in the ROI. The initial time is identified by $t_0 = 0$, whereas the manoeuvring time can be chosen arbitrarly. Without loss of generality, for this problem the final time is initially set equal to one orbital period, therefore $t_f = T_{orb}$. It is worthwhile to also define the following time vector characterizing the ROI:

$$\boldsymbol{t}^{(ROI)} = [t_0^{(ROI)} + \Delta t_0^{(ROI)}, t_0^{(ROI)} + \Delta t_1^{(ROI)}, ..., t_0^{(ROI)} + \Delta t_{n_t}^{(ROI)}] \quad (9)$$

with $\Delta t_0^{(ROI)} = 0$.

Given an inertial reference frame and a fixed body reference frame, the optimization problem here addressed can be modelled as follows:

$$\begin{aligned}
\text{Find:} \quad & J_0 = \min \sum_{i=0}^{n_t} |1 - Q(t_0^{(ROI)} + \Delta t_i^{(ROI)})| \\
& \text{subject to} \quad \forall j = 1, ..., N_F, \quad \forall t \in [t_0, t_f] \\
\text{Orbital Dynamics:} \quad & \ddot{\mathbf{r}}_j = -\frac{\mu}{r_j^3}\mathbf{r}_j + \mathbf{f}_{pert}(\mathbf{r}_j, \dot{\mathbf{r}}_j, \boldsymbol{\xi}_j, \boldsymbol{\omega}_j) \\
\text{Attitude Dynamics:} \quad & \boldsymbol{\omega}_j = \mathbf{g}(\boldsymbol{\xi}_j, \dot{\boldsymbol{\xi}}_j, \ddot{\boldsymbol{\xi}}_j); \qquad \mathbf{M}_j = \mathbf{f}(\boldsymbol{\xi}_j, \dot{\boldsymbol{\xi}}_j, \ddot{\boldsymbol{\xi}}_j); \\
\text{Initial and Final Conditions:} \quad & \mathbf{b}(\mathbf{r}_j, \dot{\mathbf{r}}_j, \boldsymbol{\xi}_j, \boldsymbol{\omega}_j) = 0; \quad \mathbf{e}(\boldsymbol{\xi}_j, \boldsymbol{\omega}_j) = 0; \\
\text{Control constraint:} \quad & p_1 \colon ||\mathbf{M}_j|| - \mathbf{M}_{max} \leq 0; \\
\text{Inter-distance constraint:} \quad & p_2 \colon ||\mathbf{r}_i - \mathbf{r}_j|| \geq \partial_{min} \qquad \forall i \neq j \in \{1, ..., N_F\}; \\
\text{Configuration Constraint:} \quad & c_1 \colon Q_{min} \leq Q(\boldsymbol{t}^{(ROI)}) \leq Q_{max} \\
& c_2 \colon \boldsymbol{\xi}_j(\boldsymbol{t}^{(ROI)}) = 0
\end{aligned} \quad (10)$$

The above parameters and relations are defined as follows:

- J_0 is the cost function to be minimized during the optimization process. The quantity that has to be reduced is given by the difference between the desired ideal value of the quality factor ($Q(\boldsymbol{t}^{(ROI)})$) in the ROI and the real value of the quality factor evaluated for every time instant of the ROI.

- $Q(\boldsymbol{t}^{(ROI)})$ is the quality factor evaluated for all the time instants of the numerical integration in the ROI; Q_{min} and Q_{max} are the minimum and maximum admissible values in the ROI, which are set respectively to 0.9 and 1.1 (Huntington & Rao, 2008).

- $\mathbf{r}_j \in \mathbb{R}^3$ and $\dot{\mathbf{r}}_j \in \mathbb{R}^3$ are the inertial positions and inertial velocities of each satellite, whilst $\boldsymbol{\xi}_j \in \mathbb{R}^3$ is the attitude parameterization given by roll, pitch and yaw; $\boldsymbol{\omega}_j \in \mathbb{R}^3$ is the body angular velocity expressed in the body reference frame and $\mathbf{M}_j \in \mathbb{R}^3$ is the external torque for the satellites' attitude control. For abbreviation, the expression for the angular velocity as a function of the Euler angle rates are contained in $\mathbf{g}(\boldsymbol{\xi}_\mathbf{j}, \dot{\boldsymbol{\xi}}_\mathbf{j}, \ddot{\boldsymbol{\xi}}_\mathbf{j})$, whereas $\mathbf{f}(\boldsymbol{\xi}_\mathbf{j}, \dot{\boldsymbol{\xi}}_\mathbf{j}, \ddot{\boldsymbol{\xi}}_\mathbf{j})$ represents Euler's equation, which relates the torques to the attitude kinematics.

- $\mathbf{f}_{pert}$ includes all the perturbing forces that have been previously mentioned, which are considered in the orbit dynamics simulator. The information regarding the Sun and Moon's ephemerides are downloaded from the JPL HORIZONS on-line solar system data and ephemeris computation, which provides highly accurate ephemerides for solar system objects, accordingly to the epoch in which the simulation is carried out.

- The initial conditions $\mathbf{b}(\mathbf{r}_j, \dot{\mathbf{r}}_j, \boldsymbol{\xi}_j, \boldsymbol{\omega}_j)$ are set on both the inertial positions and velocities of each satellite, as well as on the attitude and angular velocity; the final conditions $\mathbf{e}(\boldsymbol{\xi}_j, \boldsymbol{\omega}_j)$, on the other hand, are set only on the attitude and angular velocities of the satellites.

- The control constraint is necessary to guarantee that the control law is feasible, whereas the inter-distance constraint sets a minimum safety distance

among the satellites during the manoeuvre in order to avoid any collisions. In this case ∂_{min} is set to 4 km. As far as the configuration constraints are concerned, they are set in order for the quality factor to range between the minimum and maximum values allowed in the ROI (c_1), while keeping the satellites' attitudes to a fixed and constant Earth-pointing orientation (c_2).

3. Reconfiguration Strategy

As previously stated, a Molniya type of orbit is considered as reference orbit. Being so, the pericentre of the orbit is at 6916 km from the center of the Earth, whilst the apocentre is at a distance of 46284 km. This implies that both the SRP and atmospheric drag have a certain impact on the satellites, although the atmospheric drag has a greater influence only in a limited region around the pericentre of the orbit which happens to be also the fastest one. As a consequence, satellites are affected by drag for a brief amount of time in such a region compared to the time of the SRP influence.

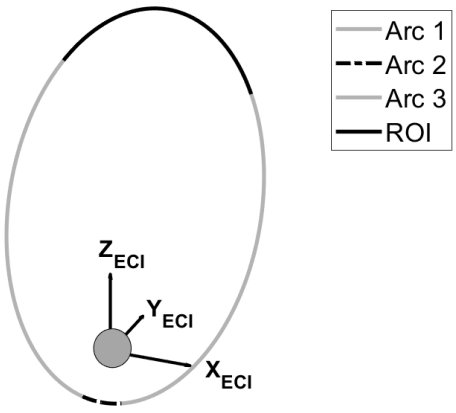

Figure 4: Molniya reference orbit: arcs division.

As anticipated in the previous section, the manoeuvring time is set to one

orbital period for simplicity, although this time can be extended to nT_{orb}, with $n = 1, 2, 3...$. The general idea is to study the control problem by dividing the reference orbit into arcs, as shown in Figure 4. One arc is designated to be the Region of Interest (ROI), defined by a range in true anomaly around the apogee of the orbit; this range is set to be of $\pm 20°$. The ROI is the portion of orbit in which the goal of the manoeuvring strategy has to be accomplished, which is to obtain a regular tetrahedron configuration. Therefore, the four satellites of the formation have to meet the configuration conditions only in this region. In the ROI the satellites' attitudes are considered fixed to an Earth-pointing orientation, as opposed to the remaining portion of orbit in which the satellites' attitudes change in order to guarantee the best exploitation of the perturbing forces, necessary to achieve the desired reconfiguration manoeuvres. Therefore, the boundary constraints on the attitude in the controlled portion of orbit are set consequently: the end and starting point of the ROI correspond respectively to the initial and final conditions for the optimization problem. The remaining part of the orbit is divided into three more arcs according to the SRP and drag effects evaluated along the entire orbit. In fact, the magnitude of the SRP effect becomes comparable to the drag from an altitude of approximately 800 km, therefore below such threshold the SRP contribution is not as strong as the drag contribution (Montenbruck & Gill, 2012): in Arc_1 and Arc_3 SRP is the main control input, whereas in Arc_2 the satellites can briefly exploit the atmospheric drag.

Table 2: Characterization of orbit's arcs division.

Orbit's region	True Anomaly (deg)	Time (hours)
Arc_1	$-160 \leq \nu \leq -23$	3.2173
Arc_2	$-23 \leq \nu \leq 23$	0.1576
Arc_3	$23 \leq \nu \leq 160$	3.2173
ROI	$160 \leq \nu \leq 200$	5.4008

In Table 2 the characterization of the arcs is shown, in terms of range in true anomaly in which they are defined, and the approximate equivalent time spent in

each arc. It is noticeable how Arc_1 and Arc_3 together correspond to the largest portion of orbit, therefore making the SRP the perturbation that is mostly exploited for manoeuvring the satellites. On the other hand, Arc_2, being smaller and around the pericenter of the orbit, is the region in which the satellites spend a considerable shorter time, yet still being able to exploit the atmospheric drag. The setting on the attitude parameters consists in leaving the three angles of the attitude parametrization free to take on any value in the allowed range of values in Arc_1 and Arc_3, whereas in Arc_2 the satellites' attitudes are considered constant. By doing so, the idea of achieving reconfiguration manoeuvres by the use of differential forces is still valid; as a matter of fact, even though the attitude angles are fixed in the central arc, each satellite maintains a constant but different orientation from one another. The choice of maintaining a fixed attitude for each satellite in the central arc is due to the fact that Arc_2 is smaller compared to the other arcs, and the formation spends a shorter time span in this region in comparison to the duration of the other two arcs. Variable attitudes in this region, together with the choice of the interpolating polynomial for the attitude parameters' approximation (which will be described in detail in the next paragraphs) could cause numerical errors, since a fast dynamics is required in a very short period in comparison with the dynamics required in the first and third arcs. Therefore the simplest and most effective implementation solution consists in keeping constant attitude angles in the central arc, without compromising either the tests results or the strategy of exploiting differential forces to achieve the desired manoeuvres.

4. IPSO applied to the reconfiguration problem

The optimization problem is solved through the IPSO algorithm which is described in detail in (Spiller, 2018). In the following paragraph only the main characteristics of the method will be presented since it has been profusely discussed in the works previously mentioned. Only the main details of the method's implementation applied to the satellite formation flying reconfiguration prob-

lem addressed in this paper are presented, since it requires a slightly different approach from the application in Spiller's works.

The IPSO is based on the combination of the Particle Swarm Optimization (PSO) and the inverse dynamics approach. The PSO is a meta-heuristic optimization method based on the evolution of a fixed number of solutions called particles, allowed to move in a feasible search space thanks to a perturbation term known as velocity, which represents the rate at which the position per generation changes. As in Spiller et al. (2018), in this work the velocity term is evaluated through the local model of the PSO (Eberhart & Kennedy, 1995). Differently from the more traditional direct dynamics approaches, which would require the application of the PSO algorithm to the attitude control, through the inverse dynamics approach the PSO algorithm is applied to the attitude kinematics instead. The angular velocity of each satellite can be expressed as a function of the attitude parameters in the body reference frame, $\boldsymbol{\omega} = \mathbf{g}(\boldsymbol{\xi}, \dot{\boldsymbol{\xi}}, \ddot{\boldsymbol{\xi}})$, therefore, from the attitude kinematics it is possible to express the sum of the external torques through Euler's equation:

$$\sum \mathbf{M}_{ext} = I\dot{\boldsymbol{\omega}} + \boldsymbol{\omega} \times I\boldsymbol{\omega} = f(\boldsymbol{\xi}, \dot{\boldsymbol{\xi}}, \ddot{\boldsymbol{\xi}}). \tag{11}$$

Once the components of $\boldsymbol{\xi}$ are approximated with B-spline curves, the quantities $\dot{\boldsymbol{\xi}}$ and $\ddot{\boldsymbol{\xi}}$ are analytically evaluated, making it possible to express both the angular velocity and the external torques in a closed form.

Two main consequences come from this approach: firstly the integration of the attitude dynamics is avoided, thus reducing the already high computational costs due to the high-fidelity simulator used for simulating the orbital dynamics; secondly, the initial and final conditions on the attitude kinematics may be imposed a priori. In this way, the attitude reorientation problem is set as a sub-problem of the generic reconfiguration problem. Basically, the goal of the optimization problem is to find an optimal attitude for the satellites to take on in the controlled arcs region, and consequently the necessary torque to achieve such attitude has to be evaluated in order to obtain a configuration as close as possible to a regular tetrahedron in the ROI.

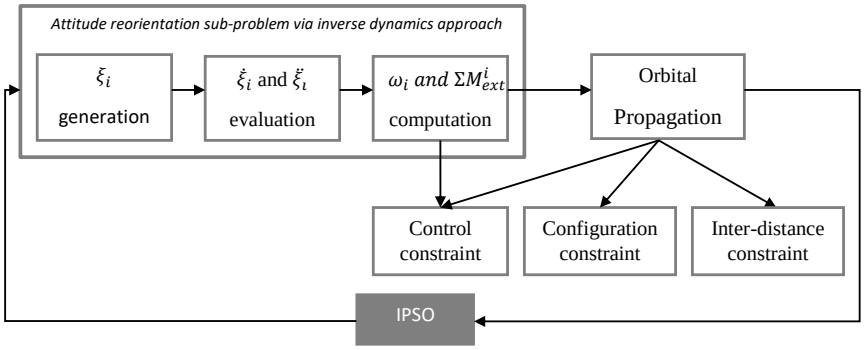

Figure 5: IPSO block diagram.

The block diagram depicted in Figure 5 shows the optimization strategy in a straightforward manner. The main steps of the algorithm can be summarized as follows:

1. each particle is associated to N_F attitude kinematics trajectories $\boldsymbol{\xi}_i \in \mathbb{R}^3, i = 1, ...N_F$, defined in the time span identified by the duration of each of the arcs in which the SRP and atmospheric drag are exploited;
2. once the attitude history is known, $\boldsymbol{a}_{SRP}$ and $\boldsymbol{a}_{Drag}$ are evaluated and the orbital dynamics integrated along the whole orbit thanks to the high-fidelity simulator;
3. the configuration in the ROI is evaluated through the quality factor and compared with the desired formation;
4. the IPSO searches for the optimal solution that guarantees a tetrahedral configuration that satisfies all the constraints reported in Eq. (10).

In order for the IPSO to stop when an optimal solution is found, an exit condition has to be defined. Usually the choice of a proper exit condition depends on the problem to solve. In this case study, given the main goal of the reconfiguration manoeuvre, the optimization process stops when it is guaranteed that the value of the quality factor evaluated in the ROI is within the maximum

and minimum admissible values, therefore this exit condition can be defined as follows:

$$\forall t \in \boldsymbol{t}^{(ROI)}$$
$$\min(Q(\boldsymbol{t}^{(ROI)})) > Q_{min}, \qquad \text{and} \qquad \max\left(Q(\boldsymbol{t}^{(ROI)})\right) < Q_{max} \tag{12}$$

where $\min(Q(\boldsymbol{t}^{(ROI)}))$ and $\max(Q(\boldsymbol{t}^{(ROI)}))$ are respectively the minimum and maximum value among the ones evaluated in the ROI, whereas $Q_{min} = 0.9$ and $Q_{max} = 1.1$ set the thresholds that define the admissible range of values that the quality factor can assume in the ROI. In addition to the exit condition, a maximum number of 3000 iterations has also been imposed in order to limit the computational time. In this way if the exit condition has not been met at the 3000^{th} iteration, the numerical simulation stops requiring therefore a different setting of the algorithm's parameters.

4.1. Attitude approximation with B-Splines

Each satellite's attitude is modelled with improved B-Spline curves, therefore the optimization parameters can be defined as:

$$\mathbf{X}_{(Arc_k)} = [\tilde{\boldsymbol{\xi}}_1^{\mathsf{T}}, \tilde{\boldsymbol{\tau}}_1^{\mathsf{T}}, ..., \tilde{\boldsymbol{\xi}}_{N_F}^{\mathsf{T}}, \tilde{\boldsymbol{\tau}}_{N_F}^{\mathsf{T}}]^{\mathsf{T}} \quad \in \mathbb{R}^{4N_F N_P} \tag{13}$$

where N_P is the number of optimization parameters that define the B-Spline curve such that $\tilde{\boldsymbol{\xi}}_i \in \mathbb{R}^{3N_P}$ and $\tilde{\boldsymbol{\tau}}_i \in \mathbb{R}^{N_P}$, with $i = 1, ..., N_F$. The definition in Eq. (13) is applied for all of the three arcs ($k = 1, 2, 3$) where the perturbations are exploited. The attitude of each satellite has been approximated considering the same B-Spline basis functions, meaning that the number of nodes, degree and length of the interpolating polynomial have been set equally for each arc. The total number of optimization parameters defined for each of the swarm's particles can be expressed as:

$$\mathbf{X} = [\mathbf{X}_{Arc_1}^{\mathsf{T}}, \mathbf{X}_{Arc_2}^{\mathsf{T}}, \mathbf{X}_{Arc_3}^{\mathsf{T}}]^{\mathsf{T}} \tag{14}$$

Thanks to the capability of B-Splines to shape curves, both the kinematic parameters (i.e roll, pitch and yaw) and the time are approximated with B-Spline

polynomials defined over the control points $\mathbf{U}_j = [\tilde{t}_j t_f, \tilde{\xi}_j]$, $j = 0, ..., N_p - 1$. The B-Spline approximation depends on a strictly increasing variable $0 \leq \lambda \leq 1$ and on the knot vector $\boldsymbol{\mathcal{K}} = [k_1 = 0 \leq k_2, ..., k_{m-1} \leq k_m = 1]^{\mathsf{T}}$, where m is a user defined value.

For each satellite, the generic component of the attitude parameters approximation vector is defined as

$$\xi_i^N(\lambda) = \boldsymbol{\mathcal{B}}(\lambda; \tilde{\boldsymbol{\xi}}, \boldsymbol{\mathcal{K}}) = \sum_{i=0}^{N_p-1} \tilde{\xi}_i N_{i,D}(\lambda; \boldsymbol{\mathcal{K}}) \tag{15}$$

whereas the time is evaluated as

$$t_i(\lambda) = t_f \boldsymbol{\mathcal{B}}(\lambda; \tilde{\boldsymbol{\tau}}, \boldsymbol{\mathcal{K}}) = t_f \sum_{i=0}^{N_p-1} \tilde{\tau}_i N_{i,D}(\lambda; \boldsymbol{\mathcal{K}}) \tag{16}$$

where the basis functions $N_{i,D}(\lambda; \boldsymbol{\mathcal{K}})$ are obtained through the Cox-de Boor recursion formula, and t_f is the reference orbital period. The definitions in Eq. (15) and (16) are also applied for each of the three arcs.

In order to guarantee an increasing total time coefficient vector, each of the time coefficient vectors in Eq. (13) needs to be correctly defined. As a consequence of this consideration and of the fact that the controlled arcs are characterized by a different time of duration, the time vectors are defined as follows:

$$\tilde{\boldsymbol{\tau}}_{i,Arc_k} = [\tilde{t}^{(1)}_{i,Arc_k}, ..., \tilde{t}^{(N_P)}_{i,Arc_k}] \cdot \alpha_{Arc_k} + \beta_{Arc_k}. \tag{17}$$

where the terms in the above equation are characterized as:

$$\begin{aligned} \tilde{\mathbf{t}}_i = &[\tilde{t}^{(1)}_{i,Arc_1} = 0, \tilde{t}^{(1)}_{i,Arc_1} < \tilde{t}^{(2)}_{i,Arc_1}, ... \\ &..., \tilde{t}^{(N_P)}_{i,Arc_1} = \tilde{t}^{(1)}_{i,Arc_2}, ..., \tilde{t}^{(1)}_{i,Arc_2} < \tilde{t}^{(2)}_{i,Arc_2}, ... \\ &..., \tilde{t}^{(N_P)}_{i,Arc_2} = \tilde{t}^{(1)}_{i,Arc_3}, \tilde{t}^{(1)}_{i,Arc_3} < \tilde{t}^{(2)}_{i,Arc_3}, ..., \tilde{t}^{(N_P)}_{i,Arc_3} = 1] \end{aligned} \tag{18}$$

with

$$\begin{aligned} \alpha_{Arc_k} &= \frac{T_{Arc_k}}{\tilde{t}^{(N_P)}_{Arc_k} - \tilde{t}^{(1)}_{Arc_k}} \\ \beta_{Arc_k} &= T - \tilde{t}^{(1)}_{Arc_k} \cdot \alpha_{Arc_k}, \end{aligned} \tag{19}$$

and

$$T = \begin{cases} 0 & k = 1 \\ T_{Arc_1} & k = 2 \\ T_{Arc_1} + T_{Arc_2} & k = 3 \end{cases} \tag{20}$$

T_{Arc_1}, T_{Arc_2} and T_{Arc_3} are the arcs' time intervals, reported in Table 2. In addition, in order to correctly define the mathematical problem, it is necessary that the approximated attitude is continuous and differentiable with respect to the time going from one arc to the next one, with at least the first time derivative continuous. In order to guarantee this, and to be coherent with the choice of maintaining a fixed attitude for each satellite in the central controlled arc (as already mentioned in the previous section), in the PSO the following conditions have been set for the optimization parameters:

$$\begin{aligned} &\tilde{\boldsymbol{\tau}}^{(1)}_{i,Arc_2} = \tilde{\boldsymbol{\tau}}^{(N_P)}_{i,Arc_1}, \quad \tilde{\boldsymbol{\xi}}^{(1)}_{i,Arc_2} = \tilde{\boldsymbol{\xi}}^{(N_P)}_{i,Arc_1}, \quad \tilde{\boldsymbol{\xi}}^{(N_p-1)}_{i,Arc_1} = \tilde{\boldsymbol{\xi}}^{(N_p-2)}_{i,Arc_1} = \tilde{\boldsymbol{\xi}}^{(1)}_{i,Arc_2}; \\ &\tilde{\boldsymbol{\tau}}^{(1)}_{i,Arc_3} = \tilde{\boldsymbol{\tau}}^{(N_P)}_{i,Arc_2}, \quad \tilde{\boldsymbol{\xi}}^{(1)}_{i,Arc_3} = \tilde{\boldsymbol{\xi}}^{(N_P)}_{i,Arc_2}, \quad \tilde{\boldsymbol{\xi}}^{(1)}_{i,Arc_3} = \tilde{\boldsymbol{\xi}}^{(2)}_{i,Arc_3} = \tilde{\boldsymbol{\xi}}^{(N_p)}_{i,Arc_2}. \end{aligned} \tag{21}$$

As far as the time derivatives of ξ^N are concerned, they can be evaluated as reported in (Spiller, 2018).

4.2. Performance Index Definition

The performance index, the penalty functions and the decreasing tolerances technique are imposed accordingly to the criterion reported in (Spiller et al., 2017b), adapting it to the problem addressed in this paper. The performance index considered can be summarized as follows:

$$J = J_0 + \sum_{i=1}^{N_c} P_i + \mu N_{vio} \tag{22}$$

where the terms P_i are the penalty functions associated with all the $N_c = 3$ constraints defined in Eq. (10), N_{vio} is the number of violated constraints and μ is a user defined weight.

The control penalty function $P_{control}$ and the inter-distance penalty function $P_{interdist}$ are evaluated for all the n_T time instants of the numerical integration

in the portion of orbit divided in the three arcs, therefore they can be expressed as:

$$P_{control} = w_{cont} \sum_{j=1}^{N_F} \sum_{k=1}^{3} \sum_{i=0}^{n_T} \beta_{j,k}(t_i) \tag{23}$$

$$P_{interdist} = w_{int} \sum_{j=1}^{N_F-1} \sum_{k=j+1}^{N_F} \sum_{i=0}^{n_T} \eta_{j,k}(t_i) \tag{24}$$

with w_{cont} and w_{int} user defined parameters, and

$$\begin{aligned} \beta_{j,k}(t_i) &= \begin{cases} 0 & \text{if} \quad \dfrac{|u_{j,k}(t_i)|}{u_{max}} - 1 < \Delta_{cont} \\ 1 & \text{otherwise} \end{cases} \\ \eta_{j,k}(t_i) &= \begin{cases} 0 & \text{if} \quad ||\mathbf{r}_j - \mathbf{r}_k|| > (1 - \Delta_{int})\delta_{min} \\ 1 & \text{otherwise} \end{cases} \end{aligned} \tag{25}$$

where $u_{j,k}$ is the component of the j^{th} satellite attitude control vector along the k^{th} body-axis, u_{max} and δ_{min} are respectively the maximum value of the admissible control and the minimum distance allowed between the formation's satellites, which is set to 4 km in accordance with the values assigned in Eq. (7). The tolerances Δ_{cont} and Δ_{int} decrease during the simulations in accordance to the scheme presented in (Spiller et al., 2017b). Regarding the configuration penalty function P_{conf}, it is evaluated for all the time instants of the numerical integration in the ROI previously described in Eq. (9), and it is defined as:

$$P_{conf} = w_Q \sum_{i=0}^{n_t} \lambda(t_i) \tag{26}$$

with $t_i \in \boldsymbol{t}^{ROI}$, and

$$\lambda(t_i) = \begin{cases} |Q(t_i) - Q_{ideal} - \Delta_Q| & \text{if} \quad |Q(t_i) - Q_{ideal}| > \Delta_Q \\ 0 \quad \text{otherwise} \end{cases} \tag{27}$$

Similarly to Eq. (23) and (24), w_Q is a user defined parameter, Δ_Q is a decreasing tolerance on the configuration evaluation and Q_{ideal} is the ideal value that the quality factor should have in the ROI, which is set to 1 according to the geometric parameter that was chosen to characterize the formation's regularity.

5. Numerical Results

The numerical simulations aim to demonstrate the feasibility of the reconfiguration manoeuvre approach that has been presented, by considering a degraded tetrahedral formation as initial condition of the optimization problem.

Table 3: Satellite parameters

Parameter	Value
Central body mass	90 kg
Lateral panel mass	40 kg
Maximum area over mass ratio	0.1529 m^2/kg
Drag coefficient C_D	2.2
Inertia tensor $I_{x,\mathcal{B}}$	$1.28 \cdot 10^3$ kg·m^2
Inertia tensor $I_{y,\mathcal{B}}$	$6.41 \cdot 10^1$ kg·m^2
Inertia tensor $I_{z,\mathcal{B}}$	$1.23 \cdot 10^3$ kg·m^2
Solar reflectivity	1

The simulations are carried out considering the same satellite model for all the four members of the formation; the satellite's dimension is shown in Figure 3, whereas the other properties are reported in Table 3. The inertia tensor is referred to the Body reference frame and it has been evaluated under the assumption of a uniformly distributed mass over the central body and panels.

Regarding the PSO settings, a swarm of 30 particles has been chosen, and the weights and initial tolerances as reported in Table 4.

Table 4: PSO parameters

Parameter	Value	Parameter	Value
w_{cont}	10^3	Δ_{cont}	0.25
w_{int}	10^3	Δ_{int}	0.25
w_Q	10^4	Δ_Q	0.3

All of the B-Spline curves used for the attitude approximation are built considering a number of $N_P = 6$ control points and polynomials of degree 6, therefore a knot vector of $m = 12$ knots. Considering the formation of $N_F = 4$

satellites, $N_P = 6$ multiplied by the number of arcs in which the perturbations are exploited (i.e. 3), three DOF for the attitude manoeuvres and the time vectors, the total number of optimization variables associated to each particle is 280, having also considered that the initial and final conditions are set a priori.

The attitude of each satellite is defined by the orientation of the body reference frame with respect to the LVLH reference; the nominal orientation in the ROI is characterized by having the $x_{\mathcal{B}}$ axis aligned with the $y_{\mathcal{L}}$ axis, the $y_{\mathcal{B}}$ axis aligned with the $z_{\mathcal{L}}$ axis, therefore the $z_{\mathcal{B}}$ axis orientated consequently. Rotation limitations are set to $\pm 90°$ per axis, with the exception of rotations around the $z_{\mathcal{B}}$ axis which are limited to $\pm 180°$. The maximum value of the admissible torque is set to $M_{max} = 10^{-3}$ N·m.

Regarding the satellites' orbital dynamics integration, a Gauss-Jackson scheme is chosen to fulfil the task with a 60-second step and the relative and absolute tolerances set to 10^{-13} and 10^{-15} respectively. In addition to using the Gauss-Jackson scheme, the efficiency of the numerical computation is improved by using the Parallel Computing utility available in Matlab: the swarm's particles are divided among the different processes where the individual best may be updated; it is only after all the particles of the current iteration are evaluated that the global and local best are calculated.

Unless differently specified, the starting epoch of the simulations are set to the date 01/01/2000 at 00:00:00 UTC, with the mesocentre of the formation starting point set to an initial true anomaly of $\nu_0 = 200°$.

5.1. Preliminary analysis

As a preliminary analysis, the satellites' orbital dynamics was integrated for a period of 10 orbits, considering a fixed Earth-pointing attitude, in order to evaluate how the formation would evolve and change along the reference orbit, without pursuing any kind of reconfiguration manoeuvre. The four satellites' initial conditions, in terms of orbit element differences (Schaub & Junkins, 2005), are listed in Table 5, which correspond to a quasi-regular tetrahedron configuration characterized by a quality factor of value $Q = 0.9609$.

Table 5: Satellites' initial conditions for Q = 0.9609

	δa(km)	δe	δi(deg)	δM_0(deg)	$\delta\Omega$(deg)	$\delta\omega$(deg)
Sat_1	$-1.29e^{-6}$	$2.13e^{-8}$	$-1.27e^{-14}$	$-1.19e^{-2}$	0	$1.02e^{-2}$
Sat_2	$2.44e^{-5}$	$1.84e^{-8}$	$-7.15e^{-3}$	$3.99e^{-3}$	0	$-3.41e^{-3}$
Sat_3	$2.42e^{-5}$	$-1.88e^{-4}$	$3.57e^{-3}$	$3.99e^{-3}$	0	$-3.42e^{-3}$
Sat_4	$2.46e^{-5}$	$1.88e^{-4}$	$3.57e^{-3}$	$3.99e^{-3}$	0	$-3.41e^{-3}$

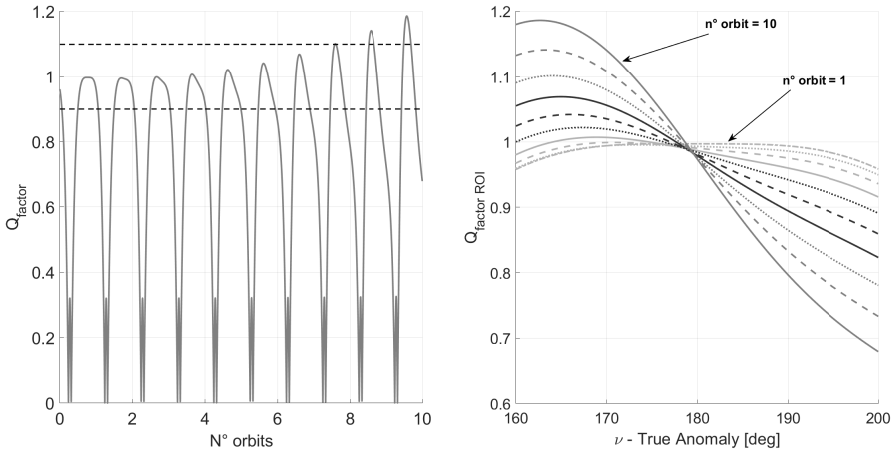

Figure 6: $\mathbf{Q_{factor}}$ evolution over a period of 10 orbits

On the left side of Figure 6 it is possible to see how the quality factor evolves in time through the 10 orbits, whilst, on the right side of the same figure, the evolution of the quality factor in the ROI is shown in function of the number of orbits along its true anomaly. It is noticeable how from orbit $n°8$ the quality factor in the ROI no longer meets both the minimum and maximum tolerances on its value, hence two possible approaches arise: one consists in controlling the satellite every time that the formation leaves the ROI therefore performing maintenance manoeuvres; a second approach is to actively manoeuvre the satellites only when the conditions on the formation are no longer admissible. The latter approach is the one analyzed in this paper, as an example of reconfiguration manoeuvre, having considered as initial conditions the ones obtained from the preliminary analysis corresponding to the satellites' position and velocity

after the 8^{th} orbit.

5.2. Reconfiguration manoeuvre over one orbit

The initial conditions of the four satellites at the beginning of the reconfiguration manoeuvre (i.e. $\nu_0 = 200°$) were deducted by the analysis carried out in the previous section, and they correspond to a degraded tetrahedral formation with a quality factor of $Q = 0.7805$. Many numerical simulations have been conducted by modifying several parameters, not only the software settings but also the orbit orientation with respect to the Sun together with the satellites' characteristics.

The first simulations were carried out considering as initial date and time January 2000 at 00:00:00 UTC. All the results that were obtained even by considering different PSO parameters settings, presented the same outcome: the reconfiguration manoeuvres did not satisfy the minimum requirements on the quality factor in the ROI. After excluding a bad setting on the algorithm parameters for the undesired outcome, the next step consisted in changing the orbit orientation with respect to the Sun, as the SRP is the perturbation mostly exploited for the passive manoeuvres. These simulations were achieved by either changing only the date of manoeuvre, maintaining all the other parameters and orbital characteristics the same, or by considering different values for the orbit's right ascension of the ascending node (RAAN), keeping the other parameters equal to the original settings.

Four different dates of execution of the manoeuvres were considered, chosen with a gap of three months apart. From the numerical simulations it resulted that only in two of these periods the reconfiguration manoeuvre is able to meet the formation requirements in the ROI. These results are represented in Fig. 7, where the trend of the Q factor in the ROI is shown for all the four dates considered, and in Table 6 where the minimum and maximum values of the Q factor evaluated in the ROI are reported.

From the results it appears that the Sun's position with respect to the orbit, and therefore of the satellite, influences the manoeuvre outcome, resulting in

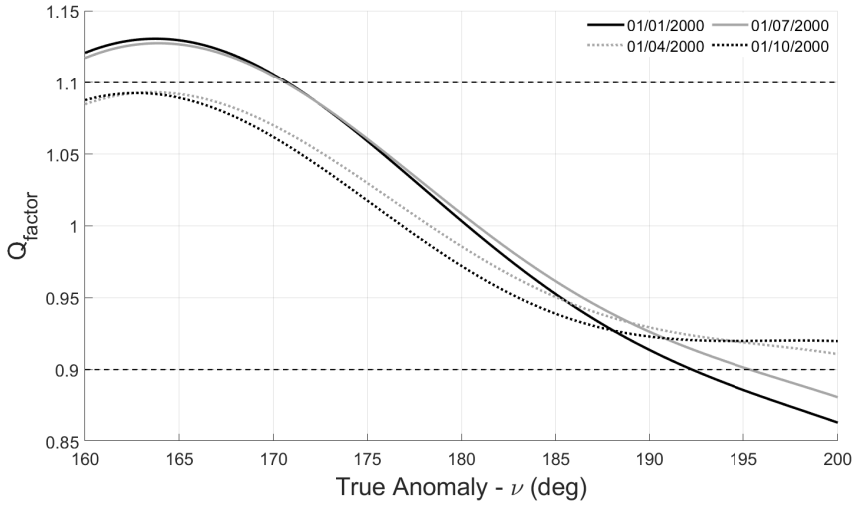

Figure 7: Comparison of the $\mathbf{Q_{factor}}$ in the ROI in different time periods after one orbit

Table 6: Min and max value of the $\mathbf{Q_{factor}}$ evaluated in the ROI in the four reference dates

Parameter	01/01/2000	01/04/2000	01/07/2000	01/10/2000
$\min Q(t_{ROI})$	0.8609	0.9081	0.8807	0.9198
$\max Q(t_{ROI})$	1.1307	1.0917	1.1276	1.0925

what it seems as an environmental limit to the manoeuvre, for the case here presented. From the reported values, the manoeuvres that satisfy the configuration requirements are the ones achieved in April and October, which corresponds to the case when the line of nodes is aligned or almost aligned with the Earth-Sun direction. Such results are also consistent with the results obtained from the simulations carried out considering the same initial date, but a RAAN of 90° and 270° instead of the original RAAN of 0°. The explanation for such an outcome is given by the fact that even though the satellites are controlled on three-axes, which means that they can be oriented with respect to the Sun in the best way possible along all three directions in order to exploit the SRP, the intensity of the force obtained is not enough to accomplish the necessary manouvre. This hypothesis is also backed up by the fact that by simply increasing the

solar panels' surfaces, even in the orbit's worst orientation case, the formation is able to reconfigure in order to satisfy the conditions in the ROI.

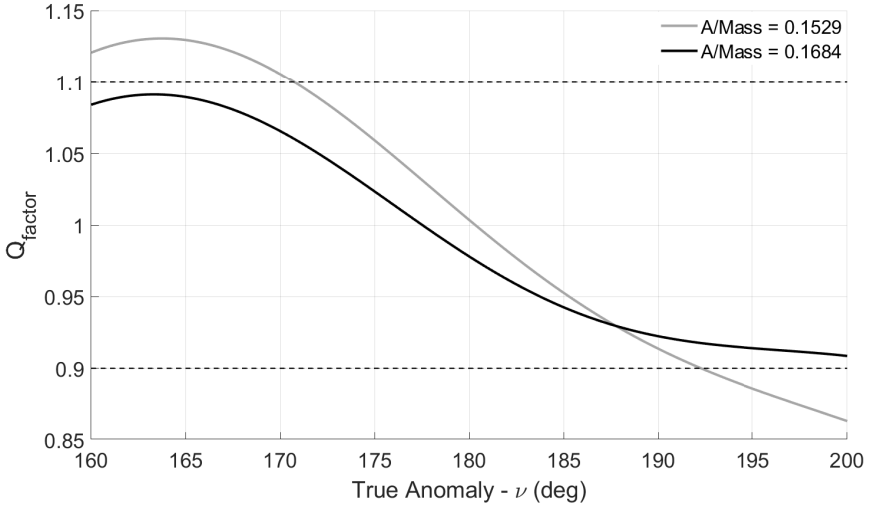

Figure 8: $\mathbf{Q_{factor}}$ in the ROI for different Area/Mass ratios at 01/01/2000

For example, by increasing the dimension of the solar panel of 1.5 m in the $y_{\mathcal{B}}$ direction, i.e. considering a 15 m^2 panel instead of a 12 m^2, the maximum Area to Mass ratio of the satellite increases from the value of $0.1529 \frac{m^2}{kg}$ to the value of $0.1684 \frac{m^2}{kg}$. Under such conditions, the manoeuvre proves to be successful in fulfilling the configuration requirements, as it is shown in Figure 8, where the trend of the Q factor in the ROI obtained with the new satellite's characteristics is compared to the one obtained with the original satellite model. To investigate in a preliminary way the dependence of achieving a successful manoeuvre from the satellite's characteristics, an estimate of the lower bound in terms of Area to Mass ratio has been evaluated. The same epoch as the one of a successful manoeuvre is considered. The simulation was carried on by testing four lower values of the Area to Mass ratio.

In Figure 9 it is possible to see the trend of the Q factor in the ROI for the four different cases. As it is possible to see, only one of the four values of the Area to Mass ratio (A/M = 0.1444 represented by the gray continuous line)

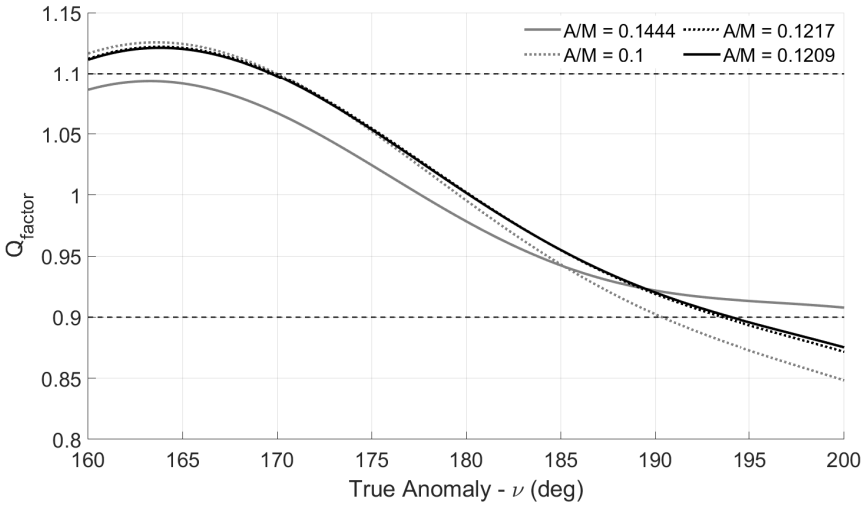

Figure 9: $\mathbf{Q_{factor}}$ in the ROI for different Area/Mass ratios at 01/04/2000

permits to satisfy the requirements on the Q factor in the ROI.

In order to demonstrate the feasibility of the proposed manoeuvring strategy, only the results of one of the successful manoeuvres are presented, specifically the results referred to the simulations executed considering 01 April 2000 as initial date at 00:00:00 UTC and the original setting on the satellite model (i.e. Area to Mass ratio of $0.1529 \frac{\mathrm{m}^2}{\mathrm{kg}}$).

The attitude history that guarantees the successful outcome of the reconfiguration manoeuvres is shown in Figure 10, whereas in Figure 11 the trends of the normalized external torques required to optimally orient the satellites are shown. It is noticeable how the values of the required torques go to zero during the time corresponding to the middle arc, coherently with the choice of keeping a fixed attitude in this portion of orbit.

An idea of the entity of the achieved manoeuvre is appreciable in Figure 12: the relative trajectories of the four satellites are represented in the LVLH reference frame. The trajectories obtained by a successful manoeuvre are represented by the grey continuous line, which are compared to the trajectories obtained without considering an optimal attitude reorientation for reconfigura-

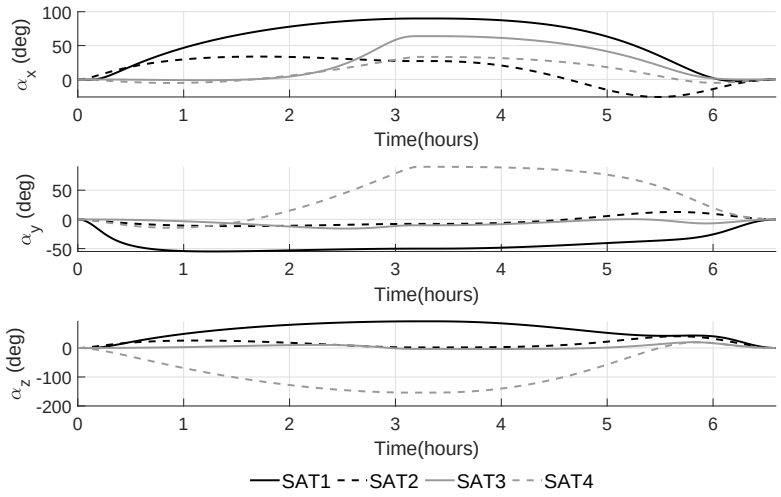

Figure 10: Rotation angles history

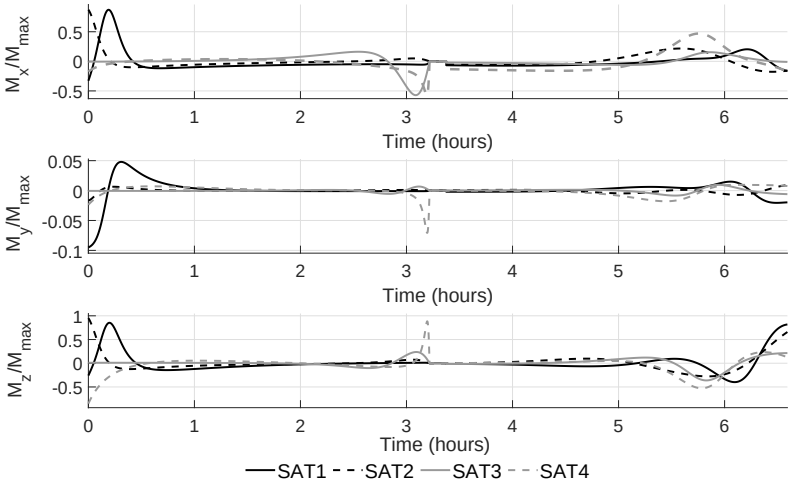

Figure 11: Required torque history

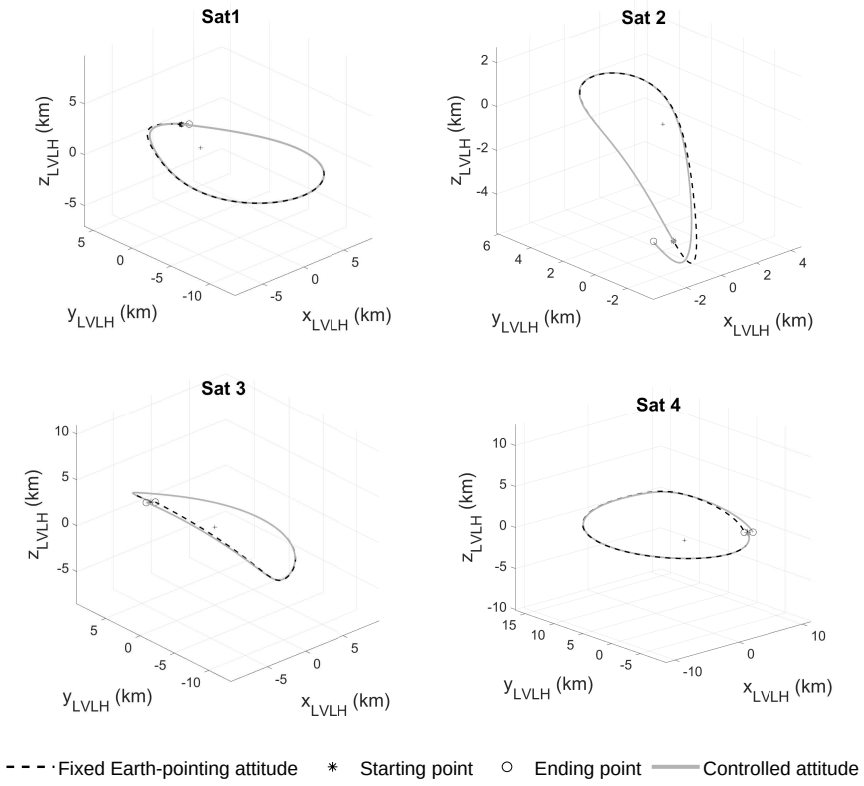

Figure 12: Relative Trajectory in the LVLH reference frame

tion manoeuvres, but by keeping the attitude fixed to an Earth-pointing orientation represented by the dashed black line. The starting and ending points are depicted so as to have an idea on the formations' changes after one orbit of manoeuvre. These observations are more evident in the projections of these trajectories; as an example the projection of the relative trajectory of Satellite 2 is reported in Figure 13.

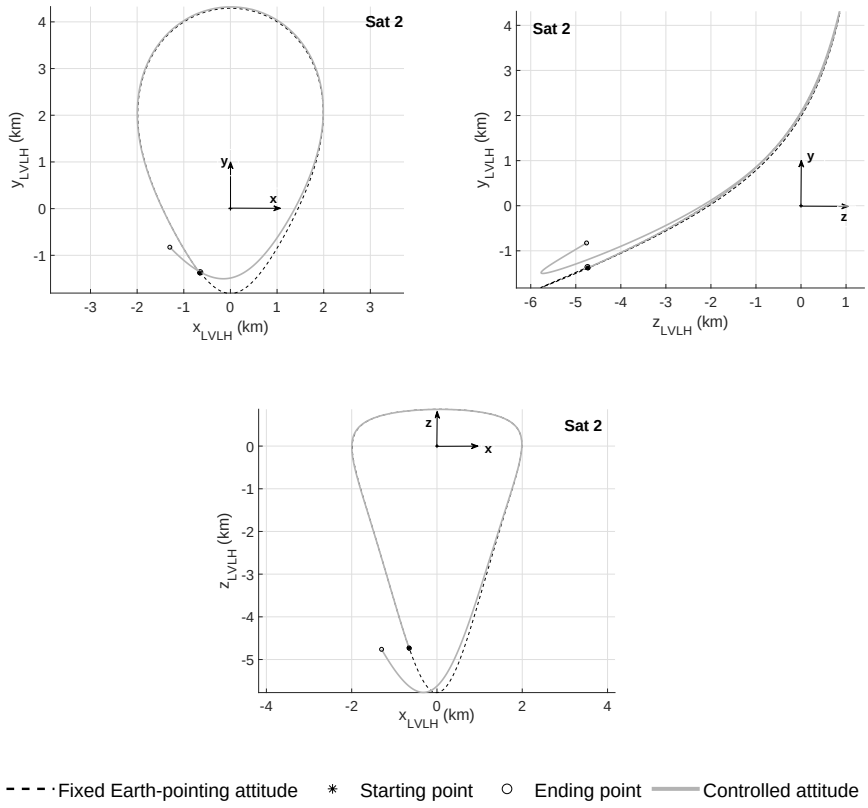

Figure 13: Relative Trajectory Projections in the LVLH reference frame

The specific forces due to drag and SRP acting on the four satellites are reported in Figures 14 and 15. The intensity of these specific forces is quite small: absolute drag is of the order of 10^{-9} km/s^2 when effective in its brief period (in fact the drag evolution illustrated refers only to the period of the affected part of the orbit); the specific force due to SRP is approximately of the

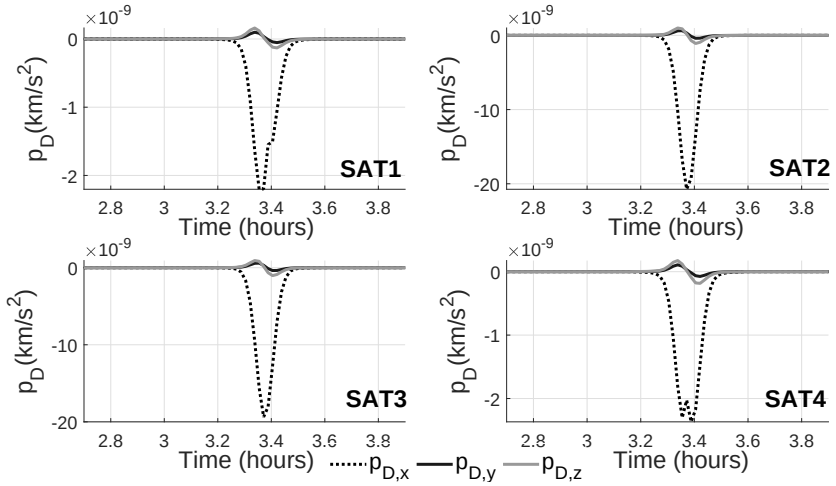

Figure 14: Drag perturbation history

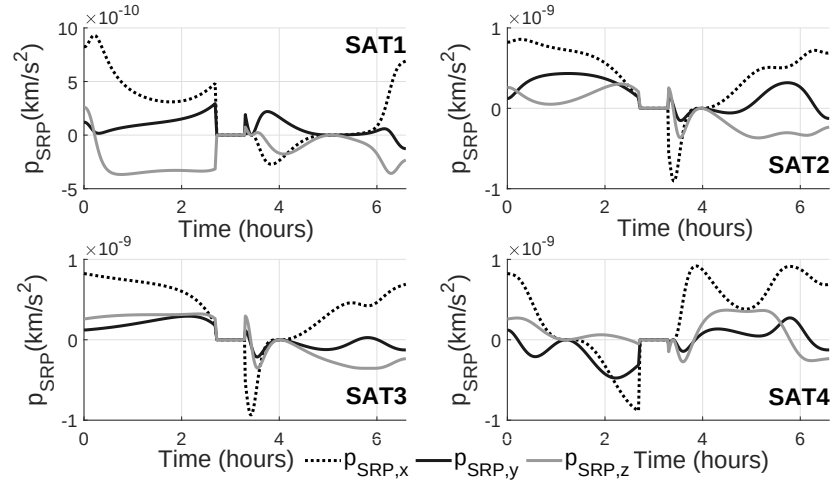

Figure 15: Solar radiation perturbation history

same order of magnitude, although it is exploited for almost all of the portion of orbit where the optimal attitude reorientation problem is studied. It is also noticeable that in correspondence with the same part of orbit, the specific SRP force goes to zero for all four satellites, which is caused by the fact that the satellites enter the Earth's shadow, since the line of nodes is almost aligned with the Sun-Earth direction.

5.3. Reconfiguration manoeuvre over two orbits

The perturbing forces can provide the satellites with small input forces, as shown in the results of the simulations presented in the previous section. Thus, it is not possible to achieve great manoeuvres unless a greater manoeuvring time is considered, or greater exposed areas are taken into account (increase in the A/m values). In fact, by considering an even more degraded initial formation ($Q = 0.7446$), which requires a greater manoeuvring effort, by conducting the simulations with the best orbit orientation, the results proved to be unsatisfactory. Preliminary results obtained by increasing the Area to Mass ratio were discussed in the previous section, therefore here the results obtained by increasing the manoeuvring time to a period equivalent to 24 hours (two times the orbital period) are presented. As expected, by extending the time in which the perturbing forces are exploited an improvement in the Q factor values is obtained, as shown in Figure 16.

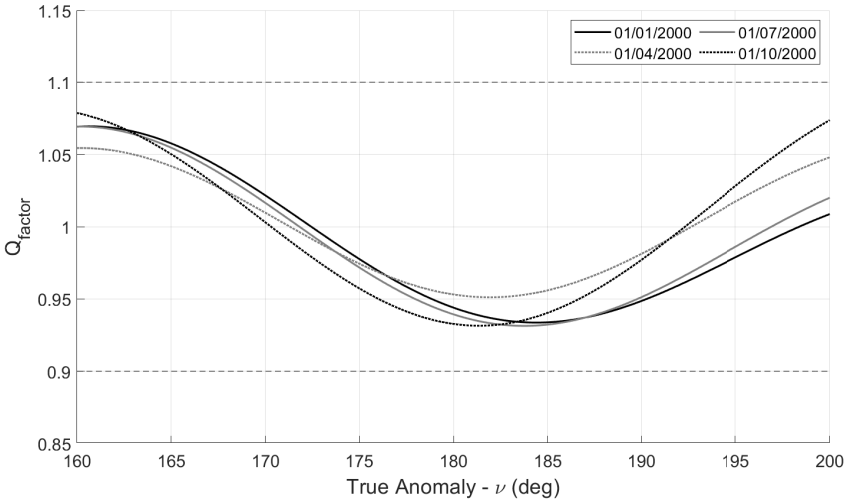

Figure 16: Comparison of the $\mathbf{Q_{factor}}$ in the ROI in different time periods after two orbits

In Table 7 the minimum and maximum values of the Q factor in the ROI obtained with an extended manoevring time are reported. Even in the cases in which the manoeuvre was not successful in Sec. 5.2, a greater manoeuvring

time allows to satisfy the requirements on the Q factor values in the ROI.

Table 7: Min and max value of the $\mathbf{Q_{factor}}$ evaluated in the ROI in the four reference dates

Parameter	01/01/2000	01/04/2000	01/07/2000	01/10/2000
$\min Q(t_{ROI})$	0.9336	0.9511	0.9313	0.9314
$\max Q(t_{ROI})$	1.0694	1.0543	1.0692	1.0786

In Figure 17 the evolution of the Q factor is shown over the number of orbits in which the manoeuvre is achieved, with reference to the case of execution of the manoeuvre set to 01/01/2000.

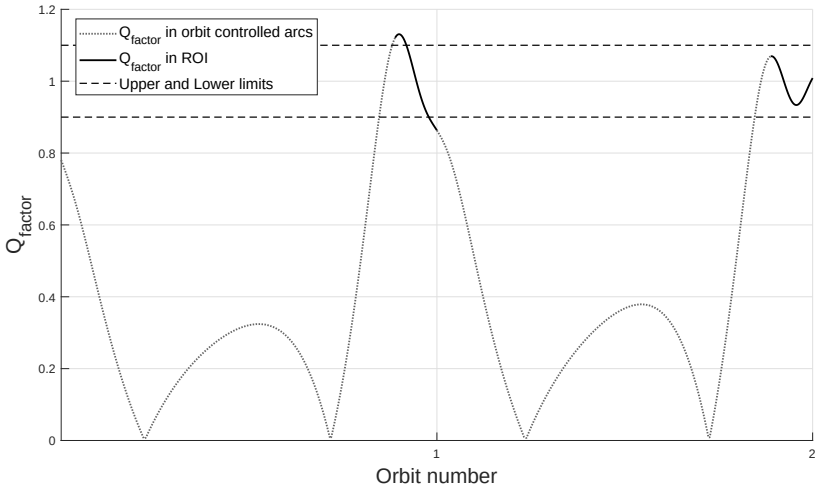

Figure 17: Quality Factor trend over a period of two orbits: 01/01/2000 case

It has been demonstrated that passive reconfiguration manoeuvres are achievable by adequately changing the satellites' attitudes under certain conditions. Limitations of such manoeuvres seemed to depend mainly on two factors, which are the orbit's orientation with respect to the Sun and the Area/Mass ratio, related to the geometrical and physical properties of the satellite's model, both of which can be overcome by increasing the time of the manoeuvres' execution.

6. Conclusion

The results presented in this paper are a consequence of a future mission concept study. The proposed approach for the planning of attitude reorientation maneouvres in order to achieve the reconfiguration of satellites in formation flying, follows the work of previously published papers (Spiller et al., 2017b) (Spiller et al., 2018). Therefore, the results obtained by the present study add new information to the feasibility of the proposed propellant-less strategy, by extending it to the case of a HEO. From the results obtained by the several simulations that have been carried out, it has been possible to highlight the possibilities and limitations concerning the proposed manoeuvring strategy, used to reconfigure a degraded tetrahedral formation into a regular one. The most important result was the successful outcome of the reconfiguration manoeuvre, meaning that the proposed strategy has proved to be possible in order to achieve a formation satisfying the imposed requirements. However, the feasibility of these manoeuvres has not always proven to be satisfactory, but it is limited by the orbit orientation with respect to the Sun and by the satellites' physical and geometrical characteristics. From the cases analyzed it resulted that the manoeuvre is favoured when the line of nodes is aligned or almost aligned with the Earth-Sun direction, whereas the worst condition is when the line of nodes is rotated of approximately 90° with respect to the Earth-Sun direction. As obviously expected, by increasing the Area to Mass ratio of the satellites, the manoeuvre resulted in being successful even in the worst orbit condition. It is most certain that the type of satellites considered influences the capability of achieving the desired manoeuvre. A rough estimation showed that the model considered for the simulations is quite close to the minimum area to mass ratio that makes it possible to satisfy the formation requirements. The initial tests that have been carried out in this study, considered a fixed manoeuvring time equivalent to one orbital period, therefore the differential accelerations were exploited only for a limited time, keeping in mind the fact that the perturbing forces are quite small in magnitude, thus providing limited manoeuvring capa-

bilities. By extending the manoeuvring time, for example to a time equivalent to two times the orbital period, an improvement on the formation's desired quality factor was registered, for both the worst and of course the best orbit orientation with respect to the Sun.

Propellant-less manoeuvring strategies such as the one proposed here, are not investigated for formation reconfiguration manoeuvres as much as their use for station keeping or rendez vous manoeuvres. The results obtained for this paper are just a contribution and an insight into what could be achieved by adopting the proposed perturbation-based reconfiguration manoeuvring approach in the field of formation flying. Being able to exploit resources that already affect the satellites in orbit, could represent a great advantage for future missions, making it a subject worthy of further studies.

References

Alfriend, K., Vadali, S. R., Gurfil, P., How, J., & Breger, L. (2009). *Spacecraft formation flying: Dynamics, control and navigation* volume 2. Elsevier.

Armellin, R., Massari, M., & Finzi, A. E. (2004). Optimal formation flying reconfiguration and station keeping maneuvers using low thrust propulsion. In *Proceedings of the 18th International Symposium on Space Flight Dynamics (ESA SP-548)* 548 (pp. 429–434).

Bruno, M. J., & Pernicka, H. J. (2005). Tundra constellation design and stationkeeping. *Journal of spacecraft and rockets*, *42*, 902–912.

Eberhart, R., & Kennedy, J. (1995). A new optimizer using particle swarm theory. In *Micro Machine and Human Science, 1995. MHS'95., Proceedings of the Sixth International Symposium on* (pp. 39–43). IEEE. doi:10.1109/MHS.1995.494215.

Guzman, J., & Schiff, C. (2002). A preliminary study for a tetrahedron formation: quality factors and visualization. In *AIAA/AAS Astrodynamics Specialist Conference and Exhibit* (p. 4637). doi:10.2514/6.2002-4637.

Hou, Y.-G., Zhang, M.-J., Zhao, C.-Y., & Sun, R.-Y. (2016). Control of tetrahedron satellite formation flying in the geosynchronous orbit using solar radiation pressure. *Astrophysics and Space Science*, *361*, 144. doi:10.1007/s10509-016-2732-1.

Hughes, S. P. (2003). Formation tetrahedron design for phase i of the magnetospheric multiscale mission, . https://ntrs.nasa.gov/search.jsp?R=20040081251.

Huntington, G. T., & Rao, A. V. (2008). Optimal reconfiguration of spacecraft formations using the gauss pseudospectral method. *Journal of Guidance, Control, and Dynamics*, *31*, 689–698. doi:10.2514/1.31083.

Ivanov, D., Mogilevsky, M., Monakhova, U., Ovchinnikov, M., & Chernyshov, A. (2018). Deployment and maintenance of nanosatellite tetrahedral formation flying using aerodynamic forces. In: International Astrinautical Congress - 2018, At Bremen, Germany.

Konstantinov, M., & Obukhov, V. (2005). Spacecraft station-keeping in the molniya orbit using electric propulsion. In *56 th International Astronautical Congress*.

Kumar, B. S., Ng, A., Yoshihara, K., & De Ruiter, A. (2011). Differential drag as a means of spacecraft formation control. *IEEE Transactions on Aerospace and Electronic Systems*, *47*, 1125–1135. doi:10.1109/TAES.2011.5751247.

Kumar, K. D., Misra, A. K., Varma, S., Reid, T., & Bellefeuille, F. (2014). Maintenance of satellite formations using environmental forces. *Acta Astronautica*, *102*, 341–354.

Li, H., & Williams, T. (2006). Reconfiguration of sun-earth libration point formations using solar radiation pressure. *Journal of spacecraft and rockets*, *43*, 1328–1339. doi:10.2514/1.16348.

Mailhe, L., Schiff, C., & Hughes, S. (2000). Formation flying in highly elliptical orbits initializing the formation, . https://ntrs.nasa.gov/search.jsp?R=20000085955.

Mashtakov, Y., Ovchinnikov, M., Petrova, T., & Tkachev, S. (2018). Attitude and relative motion control of satellites in formation flying via solar sail with variable reflectivity properties.

Montenbruck, O., & Gill, E. (2012). *Satellite orbits: models, methods and applications*. Springer Science & Business Media. doi:10.1007/978-3-642-58351-3.

Oliveira, T. C., & Prado, A. (2015). Evaluating orbits with potential to use solar sail for station-keeping maneuvers. *Adv Astronaut Sci*, *153*, 1699–1718.

Parsay, K., & Schaub, H. (2017). Drift-free solar sail formations in elliptical sun-synchronous orbits. *Acta Astronautica*, *139*, 201–212. doi:10.1016/j.actaastro.2017.06.027.

Parsay, K., Schaub, H., Schiff, C., & Williams, T. (2018). Improving magnetosphere in situ observations using solar sails. *Advances in Space Research*, *61*, 74–88. doi:10.1016/j.asr.2017.07.045.

Reid, T., & Misra, A. K. (2011). Formation flight of satellites in the presence of atmospheric drag. *Journal of Aerospace Engineering*, *3*, 64. doi:10.7446/jaesa.0301.05.

Schaub, H., & Junkins, J. L. (2005). *Analytical mechanics of space systems*. American Institute of Aeronautics and Astronautics. doi:10.2514/4.105210.

Shahid, K., & Kumar, K. (2010). Formation control at the sun-earth l2 libration point using solar radiation pressure. *Journal of Spacecraft and Rockets*, *47*, 614–626.

Shahid, K., & Kumar, K. D. (2014). Multiple spacecraft formation reconfiguration using solar radiation pressure. *Acta Astronautica*, *103*, 269–281. doi:10.1016/j.actaastro.2014.05.021.

Spiller, D. (2018). *Optimal Control Problem Solved via Swarm Intelligence*. Ph.D. thesis Sapienza University of Rome. http://hdl.handle.net/11573/1108486.

Spiller, D., Ansalone, L., & Curti, F. (2015). Particle swarm optimization for time-optimal spacecraft reorientation with keep-out cones. *Journal of Guidance, Control, and Dynamics*, *39*, 312–325. doi:10.2514/1.G001228.

Spiller, D., Basu, K., Curti, F., & Circi, C. (2018). On the optimal passive formation reconfiguration by using attitude control. *Acta Astronautica*, . doi:10.1016/j.actaastro.2018.01.052.

Spiller, D., & Curti, F. (2015). Inverse dynamics particle swarm optimization for nanosatellites rendezvous via differential drag. In: 3rd IAA Conference on University Satellite Missions CubeSat Workshop & International Workshop on Lean Satellite Standardization.

Spiller, D., Curti, F., & Ansalone, L. (2017a). Inverse-dynamics particle swarm optimization for spacecraft minimum-time slew maneuvers with constraints. *Aerotecnica Missili & Spazio*, *96*, 111–123. doi:10.19249/ams.v96i3.302.

Spiller, D., Curti, F., & Circi, C. (2017b). Minimum-time reconfiguration maneuvers of satellite formations using perturbation forces. *Journal of Guidance, Control, and Dynamics*, *40*, 1130–1143. doi:10.2514/1.G002382.

Traub, C., Romano, F., Binder, T., García-Almiñana, D., Rodríguez Donaire, S., Sureda Anfres, M. et al. (2018). A review and gap analysis of exploiting aerodynamic forces as a means to control satellite formation flight. In *Deutscher Luft-und Raumfahrtkongress 2018: 4.-6. September 2018 Friedrichshafen: Luft-und Raumfahrt-Digitalisierung und Vernetzung* (pp. 1–14).

Vallado, D. A. (2001). *Fundamentals of astrodynamics and applications* volume 12. Springer Science & Business Media.

Williams, T., & Wang, Z.-S. (2002). Uses of solar radiation pressure for satellite formation flight. *International Journal of Robust and Nonlinear Control: IFAC-Affiliated Journal*, *12*, 163–183. doi:10.1002/rnc.681.